Applied Magnetic Resonance
https://doi.org/10.1007/s00723-023-01578-z

Applied
Magnetic Resonance

ORIGINAL PAPER

Hyperpolarized Multi-organ Spectroscopy of Liver and Brain Using 1-^{13}C-Pyruvate Enhanced via Parahydrogen

Theresa L. K. Hune[1,2] · Salvatore Mamone[1,2] · Andreas B. Schmidt[3,4,5] · Inês Mahú[6] · Natascha D'Apolito[7] · Dirk Wiedermann[7] · Jens Brüning[6] · Stefan Glöggler[1,2]

Received: 11 May 2023 / Revised: 17 July 2023 / Accepted: 21 July 2023

Abstract

Hyperpolarization in nuclear magnetic resonance boosts the signals by several orders of magnitude. Using the singlet spin order of parahydrogen to create large non-equilibrium spin polarization is a fast approach to obtain hyperpolarized metabolites in seconds. In recent years, it has attracted particular interest in the field of biomedicine because signal-enhanced and ^{13}C-enriched metabolites allow for real-time metabolic investigations in combination with imaging in vivo. With this, metabolism can be traced and characterized with spatial selectivity in the body. Here, we introduce a method to use signal-enhanced metabolites to study multiple organs in separate injections to obtain real-time kinetics in vivo of these organs. Using hyperpolarized 1-^{13}C-pyruvate, we measured the kinetics of the conversion from pyruvate to lactate in the brain and the liver of mice. This we did by injecting the hyperpolarized pyruvate two times within half an hour and using each injection to measure the spectra of one region of interest. Organ cross-talk and especially how different organs affect each other in diseases is of major interest and poorly understood, because of the high complexity of biological systems. With the proof-of-principle study provided here, we are introducing a new tool to study organ-related interaction in vivo. It allows the characterization of different organs of the same animal within half an hour, which is enabled by the fast signal enhancement achieved with parahydrogen.

1 Introduction

Nuclear magnetic resonance (NMR) spectroscopy has a high diagnostic value and allows for the detection of metabolites and characterization of metabolism in vivo [1–4]. However, it also suffers from low sensitivity, and the tracking of metabolic kinetics in vivo is not possible with the standard approaches that require a large number of averages to obtain signals above the noise level. To overcome this

Extended author information available on the last page of the article

Published online: 09 August 2023

challenge, hyperpolarization techniques were introduced enhancing NMR signals by over four orders of magnitude [5]. Such large signal enhancements enable the study of metabolic real-time kinetic events in vivo. To do this, heteronuclei like ^{13}C are typically used, since they have the advantage of a longer relaxation time T_1 than protons, which allows for longer traceability of the metabolite in vivo—for ^{13}C typically up to several minutes [6].

There are different approaches to achieve hyperpolarization. Of those, dissolution dynamic nuclear polarization (DNP) is the most prominent hyperpolarization technique for studying metabolism in vivo. DNP uses electron polarization to enhance the signals of nuclear spins [7–9]. It has been used in clinical trials and produces highly polarized metabolites in high quantities [10–15]. However, it is a slow technique, taking tens of minutes to hours to produce hyperpolarized molecules, which appears to be a significant barrier to translation into clinical practice. Commercial DNP polarizers try to circumvent this by polarizing up to four samples at the same time [16, 17].

Parahydrogen (pH_2)-induced polarization (PHIP) is a comparably new technique in preclinical applications and offers the possibility to prepare hyperpolarized metabolites in a much shorter amount of time. In pH_2, at 20 K with 99% polarization, nearly all hydrogen molecules occupy the same spin state, offering a high degree of spin order [18–21]. This spin order is transferred to the molecule of interest by a method, which is called parahydrogen-induced polarization by means of side-arm hydrogenation (PHIP-SAH) [22]. Since its introduction in 2015 by Reineri et al., it has found broad application [23–32]. The workflow applied here is depicted in Fig. 1.

A precursor, in which the molecule of interest is linked to an unsaturated side-arm via a labile bond, is hydrogenated using pH_2 and a catalyst in acetone. Afterward, the spin order from the hydrogen nuclei is transferred to the ^{13}C of interest using a series of carefully timed radiofrequency pulses called the MINERVA (Maximizing Insensitive Nuclei Enhancement Reached Via parahydrogen Amplification) sequence [33]. In this case, the polarization is first transferred to a ^{13}C label on the double bond and from there to the 1-^{13}C of the pyruvate via the respective J-couplings, as described in [31]. After the transfer, the side-arm is cleaved by addition of a basic water solution. After a rapid evaporation of the acetone, the remaining aqueous solution is worked up by addition of a buffer to adjust the pH to physiological conditions and filtration of the hydrogenation catalyst—leading to a clean solution of the hyperpolarized metabolite in water, which can then be injected into an organism. The whole procedure from the start of hydrogenation to the injection requires typically about one minute. Once injected, the hyperpolarized spin label is visible in the NMR spectra and can be used for the localization and characterization of disease or the investigation of metabolism in vivo [34–39]. The spectra of the metabolites can either be measured over the whole body [40, 41] or selectively over a region of interest, for example a single organ [42, 43]. However, usually, a choice has to be made as to which region should be observed, because the allowed injection volume and, therefore, the sensitivity of the experiment is limited especially in preclinical studies performed on rodents. Multiple injections would provide a way to work around this limitation. In vivo studies with DNP in rodents (mostly rats)

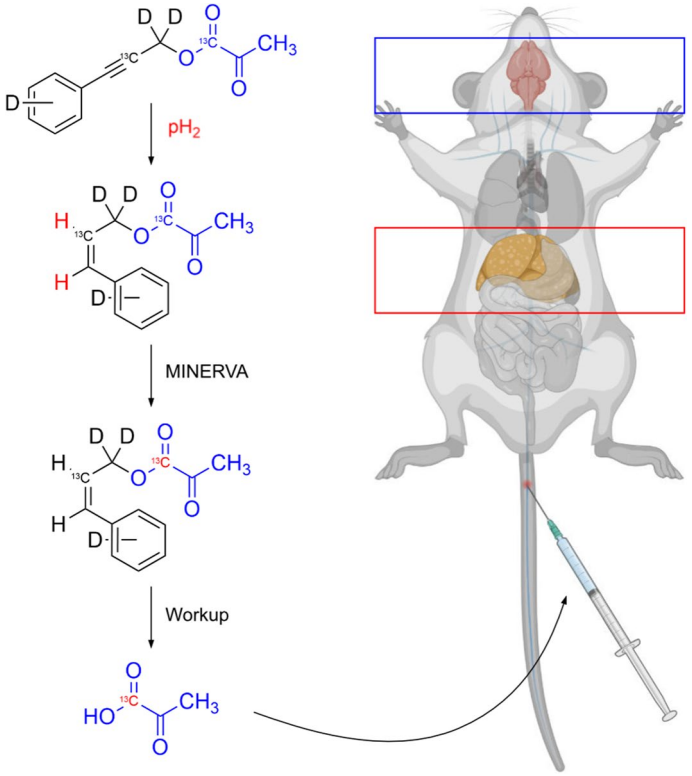

Fig. 1 Workflow for the hyperpolarization of 1-^{13}C-pyruvate with PHIP-SAH. The precursor, a phenyl propargyl ester of pyruvate, is hydrogenated using pH_2 and an Rh-catalyst. The transfer of the polarization to the 1-^{13}C with the MINERVA sequence is performed via an intermediate ^{13}C at the unsaturated bond and was described in [31]. The sequence is followed by a work-up procedure including the addition of base to cleave the ester bond, evaporation of the acetone, addition of buffer to adjust the pH, and filtration of the catalyst. The resulting aqueous solution containing the hyperpolarized 1-^{13}C-pyruvate is injected into the tail vein of the mouse. The first injection is used to measure a series of localized spectra of the brain region, while 10–25 min later, the second injection is used to take a series of spectra from the liver region. Figure was created using Biorender and Affinity Designer 2.0

demonstrated that two successive injections can be used to study the same region of interest, as to get two data points from one animal [44–46]. Studying large cohorts, however, appears to be out of reach even with multiple samples being enhanced at the same time.

This work demonstrates the possibility to study two different organs of the same animal with PHIP, using two injections of hyperpolarized 1-^{13}C-pyruvate. We recorded spectra of the region of the brain and the liver of mice within less than half an hour and analyzed them with regard to the conversion of pyruvate to lactate. Furthermore, we propose this double injection procedure for multiple organ studies over a single-dose injection, because the hyperpolarized signal could be unintentionally depleted if one excites and detects the ^{13}C spin in one organ and afterward tries to detect the metabolic conversion in a second organ.

This study demonstrates that the high throughput of hyperpolarized metabolites achieved with parahydrogen enables extensive studies of complex biological systems. With this, metabolism in different organs of the same animal can be studied simultaneously, opening possibilities to study organ cross-talk and reduce the necessary number of animals by accessing more information from each one. The method is minimally invasive, and the animals can be woken up again and used for further studies, enabling also longitudinal characterization of metabolism and disease progression.

2 Methods

2.1 On-Site Production of Parahydrogen

Molecular hydrogen was produced by an electrolysis unit (H2PEM-510, Parker Hannifin, Cleveland, Ohio) and fed directly into a parahydrogen generator (BPHG 90, Bruker Corporation, Ettlingen, Germany) at 36 K (92% para-enrichment). The parahydrogen was compressed to a pressure of 10 bar in a 1 L buffer cylinder and led to the sample through a home-built tubing system.

2.2 Hyperpolarization

All chemicals except the precursor were purchased from commercial suppliers and used as received. The synthesis for the precursor 3-(phenyl-d5)prop-2-yn-1-yl-2-13C-1,1-d2 2-oxopropanoate-1-13C as well as the full work-up procedure were described in [31]. Briefly, a solution of 13 mM rhodium catalyst, [1,4-Bis(diphenylphosphino)butane](1,5-cyclooctadiene)rhodium(I) tetrafluoroborate (Sigma-Aldrich 79255-71-3, $M = 724.4$ g/mol) and 95 mM of the precursor in acetone-d6 was prepared. For each sample, 200 µL of this solution were filled into an 8-inch 5 mm NMR tube. The hyperpolarization procedure was performed using a home-built electromagnet operating at 21.5 mT. The samples were degassed by bubbling nitrogen gas through the solution prewarmed in a water bath at 80 °C for about 2 min. Afterward, the NMR tubes were placed inside a custom-built dual channel probe in the bore of the electromagnet for the PHIP experiments. A more detailed description of the system is given in [27, 31].

Parahydrogen was bubbled through the sample at a pressure of 7 bar for 15 s. Following the hydrogenation, the MINERVA pulse sequence was used to transfer the polarization from the protons to the ^{13}C of interest, in this case the 1-^{13}C of the pyruvate moiety [33].

After pressure release, a solution of 100 mM Na_2CO_3 in water was added to cleave the ester bond. The acetone was removed by evaporation through flushing with nitrogen gas at a pressure of 8 bar and the pH was adjusted to physiological conditions using 1X PBS-buffered saline at pH 1.1. The catalyst precipitates after the evaporation of the acetone forming large coagulates and was then removed by passing the solution through a membrane filter with a 1.0 µm pore size. The aqueous

solution containing clean hyperpolarized pyruvate was ready to be injected. A more detailed description on the procedure was previously described [31–33].

2.3 Animal Housing and Mouse Handling

Experiments were carried out in accordance with the EU directive 2010/63/EU for animal experiments and the German Animal Welfare Act (TierSchG, 2006) and were approved by the regional authorities (LANUV NRW; application number 81-02.04.2020.A157). Animals used in this study were housed under standard laboratory conditions in a 12 h light cycle with food and water available ad libitum and kept in groups of up to five. The mice were between 3 and 4 months old and fed a high-fat diet. Male mice ($n = 3$) with a C57BL/6 N genetic background were used for the measurements.

The mice were anesthetized in a dedicated container using 4% isoflurane in O_2 and N_2O (1:3). Afterward, the isoflurane was decreased and kept between 2 and 3% for the whole measurement. A tail vein catheter was placed and the mice were positioned head-prone on a custom-built warming water mat to ensure constant body temperature. Body temperatures as well as breathing rates were monitored during the anesthesia. The mice were positioned inside the coil alongside a urea phantom, used as a reference for the ^{13}C chemical shift scale, so that both the brain and the liver were inside the sensitive volume.

2.4 MR Measurements

All measurements were performed in a 9.4 T preclinical Bruker MR scanner (Bruker Corporation, Ettlingen, Germany) equipped with a 13C/1H Volume Coil by RAPID Biomedical (RAPID Biomedical GmbH, Rimpar, Germany). Localized spectroscopy of the brain region and the liver region was performed with a standard spectroscopy sequence from Bruker (NSPECT) with axial slice selection. The slices were positioned using anatomical proton images for reference, so that the respective slice included the complete organ, resulting in a slice thickness for the brain of 18 mm and for the liver of 21 mm. For each measurement, a series of 128 spectra were recorded with a flip angle of 18° and TR = 2 s, resulting in a measurement time of about 4 min. The acquisition was started prior to injection to record the increase of the NMR signal following pyruvate uptake in the organ of interest. The reference power for protons was adjusted automatically. The reference power for carbon was determined to be 0.19 W. The pulse duration for the spectroscopy on carbon was set to 0.2 ms. The anatomical proton images were recorded using a Bruker standard FLASH sequence with coronal and sagittal slice orientation. The number of slices was 70 with a slice thickness of 1 mm and the matrix size was 256 × 256 in an 80 mm × 80 mm FOV.

Each mouse was injected twice with independently generated hyperpolarized substrate. For each measurement, 2.5 µL/g of body weight of pyruvate solution (40 mM) was injected through a catheter into the lateral tail vein of the mouse. The first measurement was performed on the brain, and the second on the liver. The time

between the two injections was kept below half an hour. Each mouse was kept no longer than 2 h under anesthesia. After the experiment, the mice were woken up.

2.5 Data Analysis

The data analysis is described in detail in [41]. The spectra were processed using TopSpin 4.0. Phase correction as well as line broadening and baseline correction were applied. All further analysis was performed using Python 3.0 in Jupyter Notebooks. In each spectrum, the peaks of pyruvate and lactate were integrated and summed up to determine the area under the curves (AUCs).

Following the procedure described by Hill et al. [47], from the ratio of the AUCs, the rate constant k_{PL} was calculated using Eq. (1), under the assumption that the back conversion is negligible ($k_{LP}=0$), which is usually justified because of the low lactate levels [48]

$$\frac{\mathrm{AUC(L)}}{\mathrm{AUC(P)}} = \frac{k_{PL}}{\frac{1}{T_1(L)} + k_{LP}}. \tag{1}$$

To do this, an effective T_1 of pyruvate and lactate had to be estimated according to the literature values [49, 50] and taking into account the loss of polarization due to rf pulses. The values used were $T_1(P)=25$ s, $T_1(L)=20$ s.

To visualize the results and evaluate the quality of the determined rate constant as well as the estimated value for T_1, the lactate curve was recalculated using those parameters as described in [33]. For this, the rate laws for the pyruvate as well as the lactate signal were formulated as follows:

$$\frac{\mathrm{d[L](t)}}{\mathrm{dt}} = k_{PL} \cdot [\mathrm{P}](t) - \left(\frac{1}{\mathrm{T_1(L)}} + k_{LP}\right) \cdot [\mathrm{L}](t) \tag{2}$$

$$\frac{\mathrm{d[P](t)}}{\mathrm{dt}} = -k_{PL} \cdot [\mathrm{P}](t) + \left(\frac{1}{\mathrm{T_1(P)}} + k_{LP}\right) \cdot [\mathrm{L}](t). \tag{3}$$

This set of differential equations was solved to obtain [L](t) by providing the data points of both pyruvate and lactate at the pyruvate maximum as initial conditions, as well as the k_{PL} determined with Eq. (1) and the estimated T_1 times.

To make sure that the assumption of $k_{LP}=0$ is justified, the lactate curve was also modeled with $k_{LP}=k_{PL}/5$. The recalculated lactate data are plotted in Fig. 3.

3 Results and Discussion

Figure 2 shows the ^{13}C-NMR spectrum of the hyperpolarized pyruvate, measured in the low-field spectrometer directly after parahydrogen bubbling and application of the polarization transfer sequence. Below the pyruvate spectrum, the ^{1}H-spectrum of water acquired at the same Larmor frequency (~230 kHz) using 2000 scans is

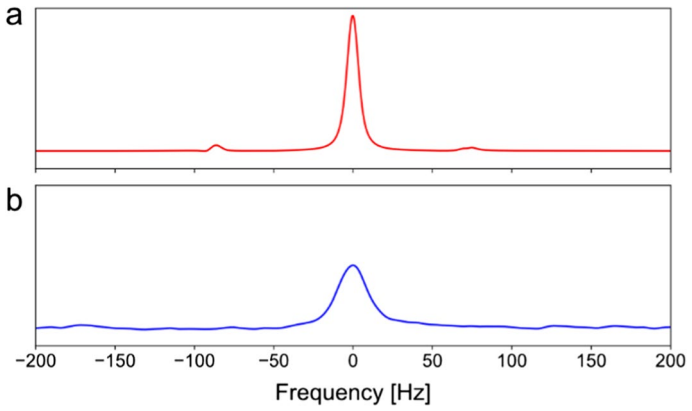

Fig. 2 Spectra of hyperpolarized pyruvate and reference spectrum of water measured using the 21.5 mT electromagnet. The spectrum in **a** shows the ^{13}C-NMR spectrum of 40 mM hyperpolarized 1-^{13}C-pyruvate after hydrogenation and polarization transfer acquired with one scan at 21.5 mT (Larmor frequency ~ 230 kHz). The spectrum **b** shows the thermal ^{1}H-spectrum of 200 µL H_2O acquired at 293 K with 2000 scans on the same coil and frequency of spectrum in (**a**) at 5.69 mT. The signal of the pyruvate is enhanced by a factor of 7.7 million, which corresponds to a polarization of ~ 14.5%

shown. Compared to thermal polarization, the signal of the pyruvate is enhanced by a factor of 7.7 million, which corresponds to a ^{13}C polarization of 14.5% at 21.5 mT. After the full work-up procedure, the concentration of the pyruvate in physiologically adjusted neat water solutions was found to be ~ 40 mM with polarization levels ~ 6.5%. This biocompatible solution was then rapidly transferred to the MRI scanner and administered into the waiting mouse.

Each mouse was injected twice with pyruvate solutions that were hyperpolarized directly before each injection. The first injection was used to record a series of spectra of the brain, while the second one was used to record a series of spectra over the liver region. Figure 3a shows the positioning of the slices for one representative mouse. After injection, the influx of pyruvate became quickly visible in the spectra. Shortly afterward, lactate production was observed by the appearance of the corresponding signal. From the recorded spectra, the pyruvate as well as the lactate peaks were integrated and the curves are plotted in Fig. 3b and c.

In metabolic MR studies, the ratio of the area under the curves (AUC) for the pyruvate and the lactate peak is an important parameter frequently used to characterize metabolism. This ratio correlates with the rate constant k_{PL} of pyruvate to lactate in the observed slice [47]. The AUCs were determined from the curves and the rate constants were calculated. The calculated rate constants were then used to model the lactate curve to assess the quality of the parameters with respect to the measured data. The recalculated lactate curves are plotted in Fig. 3b and c. The ratio of the AUCs as well as the k_{PL} in both organs including their standard deviations were determined from the recorded spectra, as summarized in Table 1. The recalculated curves with and without k_{LP} are in good agreement with each other.

The obtained values for the rate constants suggest the tendency of a lower lactate production in the liver than in the brain. As the mice were young (3–4 months), the

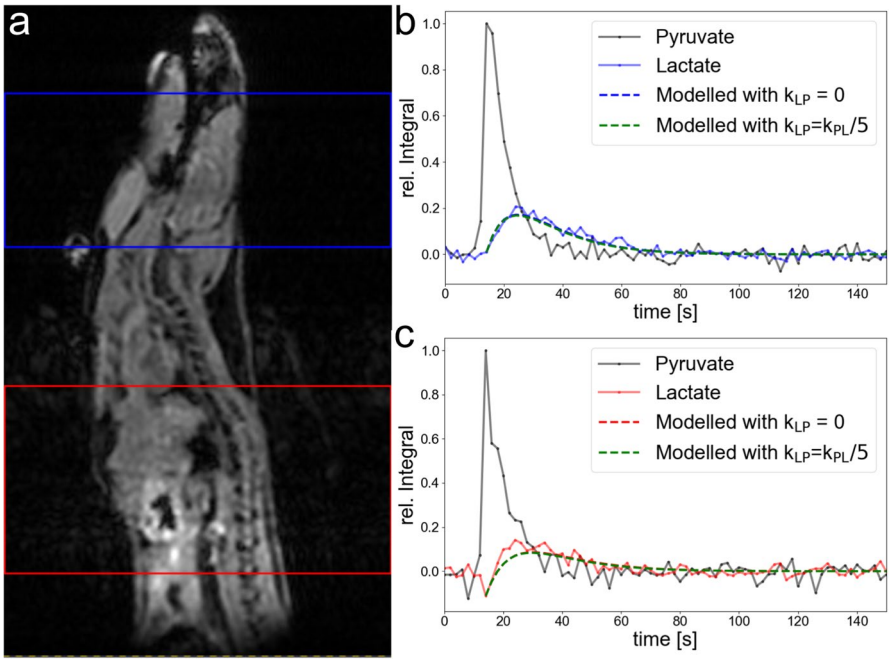

Fig. 3 Slice positions and plots extracted from the hyperpolarized ^{13}C-NMR spectra for one representative mouse. NMR spectra with a flip angle of 18° were recorded every 2 s during injection of the hyperpolarized pyruvate. From each spectrum, the pyruvate and the lactate peak were integrated and normalized to the integral of highest intensity. **a** Position of the axial slices from which the spectra were taken on top of one slice of the sagittal proton MR image. The slice over the brain (blue) has a thickness of 18 mm; the one over the liver (red) is 21 mm thick to include the whole organ. **b** Peak integrals of pyruvate (black) and lactate (blue) in the brain region plotted over time, including the model of the lactate curve based on the AUC ratio with $k_{LP}=0$ (blue) and $k_{LP}=k_{PL}/5$ (green). The recalculated data with $k_{LP}=0$ and $k_{LP}=k_{PL}/5$ show no difference. **c** Peak integrals of pyruvate (black) and lactate (red) in the liver plotted over time, including the model of the lactate curve based on the AUC ratio with $k_{LP}=0$ (red) and $k_{LP}=k_{PL}/5$ (green). The recalculated data with $k_{LP}=0$ and $k_{LP}=k_{PL}/5$ show no difference. Figure was created using Python 3.0 and Affinity Designer 2.0

Table 1 Mean and standard deviations for the ratio of the AUCs from lactate and pyruvate as well as the rate constant k_{PL} determined from the spectra

	AUC(Lac)/AUC(Pyr)	k_{PL} [s^{-1}]
Brain	0.58 ± 0.03	0.044 ± 0.003
Liver	0.38 ± 0.22	0.028 ± 0.017

low lactate levels are not surprising. However, the pyruvate-to-lactate conversion in the brain is strongly influenced by the anesthetics, i.e., isoflurane in our case. Shortly after the initiation of the narcosis, the lactate level in the brain has been shown to stabilize, but at a significantly higher level [51, 52]. This explains the elevated pyruvate-to-lactate conversion observed in the brain. Overall, the signal enhancement

and the high throughput of the method enable subsequent injections into the same animal in a short amount of time. Sufficient signal intensities are still maintained, even though the maximum possible injection volume was distributed between two injections.

4 Conclusions

In this work, we demonstrated the possibility to use two injections to investigate the metabolism of two different organs in vivo using PHIP-hyperpolarized 1-^{13}C-pyruvate. The presented results demonstrate the feasibility of this method for multi-organ studies. In particular, we believe that multiple injections have the advantage over double excitation experiments with one injection that organs can be monitored without accounting for effects due to the saturation of signal by pulses, while another organ may be investigated. Additionally, changes in pyruvate-to-lactate conversion are a biomarker for diagnosis, therapy, and treatment response in several diseases and are hence of high interest.

The presented procedure offers the possibility to investigate dependencies and cross-correlations between different regions in the body of the same animal in vivo. It paves the way for the characterization of more complex co-dependencies in disease models, also with regard to longitudinal studies. Additionally, it provides a means to reduce the number of animals used in biological studies, where often large cohorts are necessary to achieve statistical significance, and makes them available by increasing the amount of available information from one animal. Additionally, it may prove advantageous to couple the presented approach with a quasi-continuous production of contrast agents [53].

We would like to emphasize that we see the use of parahydrogen enhanced metabolites as key to enable biological studies on large cohorts, since metabolites can be rapidly generated and multiple investigations on various organs and study subjects can be carried out per day.

Acknowledgements The authors thank Vera Jörke and Dr. Andreas Schmid from WSIC in Tübingen for their help with the warming mat, as well as Ulla Uhlenküken for the support regarding the MR scanner. Furthermore, the authors thank Dr. Vladimir Belov and Jan Seikowski from the synthesis facility of the MPI-NAT as well as Mario Lengauer and Christian Klaba from the workshop for fine mechanics of the MPI-NAT. Salvatore Mamone thanks Dr. Lukas Kaltschnee (MPI-NAT) for useful discussions about the parahydrogen setup. This project has received funding from the European Research Council (ERC) under the European Union's Horizon 2020 research and innovation program (Grant Agreement No. 949180). Stefan Glöggler acknowledges funding by the Max Planck Society and the German Research Foundation (DFG) 495627437. Andreas B. Schmidt acknowledges funding support by the German Cancer Consortium (DKTK) and the DFG (#SCHM 3694/1-1, #SCHM 3694/2-1, #SFB1479). Material preparation, data collection, and analysis were performed by Theresa L. K. Hune, Salvatore Mamone, Inês Mahú, and Natascha D'Apolito. Stefan Glöggler conceived the study. The first draft of the manuscript was written by Theresa L. K. Hune and all authors commented on previous versions of the manuscript. All authors read and approved the final manuscript.

Author Contributions Material preparation, data collection, and analysis were performed by TLKH, SM, IM, and ND'A. SG conceived the study. All authors discussed the study design. The first draft of the manuscript was written by TLKH and all authors commented on previous versions of the manuscript. All authors read and approved the final manuscript.

Funding Open Access funding enabled and organized by Projekt DEAL. This project has received funding from the European Research Council (ERC) under the European Union's Horizon 2020 research and innovation program (Grant Agreement No. 949180). Stefan Glöggler acknowledges funding by the Max Planck Society and the German Research Foundation (DFG) under Grant 495627437. Andreas B. Schmidt acknowledges funding support by the German Cancer Consortium (DKTK) and the DFG (#SCHM 3694/1-1, #SCHM 3694/2-1, #SFB1479).

Data Availability The data that support the findings of the manuscript are available in the main text and can be obtained from the authors upon request.

Declarations

Conflict of Interest Stefan Glöggler is co-founder of MagniKeen. The authors declare no competing financial interests.

Ethical Approval Experiments were carried out in accordance with the EU directive 2010/63/EU for animal experiments and the German Animal Welfare Act (TierSchG, 2006) and were approved by the regional authorities (LANUV NRW; Application Number 81-02.04.2020.A157).

References

1. S.W. Provencher, Estimation of metabolite concentrations from localized in vivo proton NMR spectra. Magn. Reson. Med. **30**, 672–679 (1993)
2. M. Hajek, M. Dezortova, Introduction to clinical in vivo MR spectroscopy. Eur. J. Radiol. **67**, 185–193 (2008)
3. D. Bertholdo, A. Watcharakorn, M. Castillo, Brain proton magnetic resonance spectroscopy: introduction and overview. Neuroimaging Clin. N. Am. **23**, 359–380 (2013)
4. S. Posse, R. Otazo, S.R. Dager, J. Alger, MR spectroscopic imaging: principles and recent advances. J. Magn. Reson. Imaging **37**, 1301–1325 (2013)
5. J.H. Ardenkjær-Larsen et al., Increase in signal-to-noise ratio of > 10,000 times in liquid-state NMR. PNAS **100**, 10158–10163 (2003)
6. S. Day, M. Kettunen, F. Gallagher et al., Detecting tumor response to treatment using hyperpolarized ^{13}C magnetic resonance imaging and spectroscopy. Nat. Med. **13**, 1382–1387 (2007)
7. A.C. Pinon, A. Capozzi, J.H. Ardenkjær-Larsen, Hyperpolarization via dissolution dynamic nuclear polarization: new technological and methodological advances. MAGMA **34**, 5–23 (2021)
8. R.E. Hurd, Y.-F. Yen, A. Chen, J.H. Ardenkjaer-Larsen, Hyperpolarized 13C metabolic imaging using dissolution dynamic nuclear polarization. J. Magn. Reson. Imaging **36**, 1314–1328 (2012)
9. H. Gutte et al., The use of dynamic nuclear polarization (13)C-pyruvate MRS in cancer. Am. J. Nucl. Med. Mol. Imaging **5**, 548–560 (2015)
10. F.A. Gallagher et al., Magnetic resonance imaging of pH in vivo using hyperpolarized 13C-labelled bicarbonate. Nature **453**, 940–943 (2008)
11. S.J. Nelson et al., Metabolic imaging of patients with prostate cancer using hyperpolarized [13C] pyruvate. Sci. Transl. Med. **5**, 198ra108-198ra108 (2013)
12. J.T. Grist et al., Quantifying normal human brain metabolism using hyperpolarized [1–13C]pyruvate and magnetic resonance imaging. Neuroimage **189**, 171–179 (2019)

13. N. Bøgh et al., Imaging neurodegenerative metabolism in amyotrophic lateral sclerosis with hyperpolarized [1-13C]pyruvate MRI. Tomography **8**, 1570–1577 (2022)
14. F. Zaccagna et al., Imaging glioblastoma metabolism by using hyperpolarized [1–13C]pyruvate demonstrates heterogeneity in lactate labeling: a proof of principle study. Radiology **4**, e210076 (2022)
15. J.D. Kaggie et al., Deuterium metabolic imaging and hyperpolarized 13C-MRI of the normal human brain at clinical field strength reveals differential cerebral metabolism. Neuroimage **257**, 119284 (2022)
16. K. Golman, R. Zandt, M. Thaning, Real-time metabolic imaging. PNAS **103**, 11270–11275 (2006)
17. S. Jannin, A. Bornet, R. Melzi, G. Bodenhausen, High field dynamic nuclear polarization at 6.7T: Carbon-13 polarization above 70% within 20min. Chem. Phys. Lett. **549**, 99–102 (2012)
18. C.R. Bowers, D.P. Weitekamp, Transformation of symmetrization order to nuclear-spin magnetization by chemical reaction and nuclear magnetic resonance. Phys. Rev. Lett. **57**, 2645–2648 (1986)
19. C.R. Bowers, D.P. Weitekamp, Parahydrogen and synthesis allow dramatically enhanced nuclear alignment. J. Am. Chem. Soc **109**, 5541–5542 (1987)
20. J. Natterer, J. Bargon, Parahydrogen induced polarization. Prog. Nucl. Magn. Reson. Spectrosc. **31**, 293–315 (1997)
21. R.A. Green et al., The theory and practice of hyperpolarization in magnetic resonance using parahydrogen. Prog. Nucl. Magn. Reson. Spectrosc. **67**, 1–48 (2012)
22. F. Reineri, T. Boi, S. Aime, ParaHydrogen induced polarization of 13C carboxylate resonance in acetate and pyruvate. Nat. Commun. **6**, 5858 (2015)
23. S. Knecht et al., Rapid hyperpolarization and purification of the metabolite fumarate in aqueous solution. Proc. Natl. Acad. Sci. USA (2021). https://doi.org/10.1073/pnas.2025383118
24. E. Cavallari, C. Carrera, S. Aime, F. Reineri, Studies to enhance the hyperpolarization level in PHIP-SAH-produced C13-pyruvate. J. Magn. Reson. **289**, 12–17 (2018)
25. S. Korchak, S. Yang, S. Mamone, S. Glöggler, Pulsed magnetic resonance to signal-enhance metabolites within seconds by utilizing para-hydrogen. ChemistryOpen **7**, 344–348 (2018)
26. S. Korchak, S. Mamone, S. Glöggler, Over 50 % 1H and 13C polarization for generating hyperpolarized metabolites—a para-hydrogen approach. ChemistryOpen **7**, 672–676 (2018)
27. S. Korchak, M. Emondts, S. Mamone, B. Blümich, S. Glöggler, Production of highly concentrated and hyperpolarized metabolites within seconds in high and low magnetic fields. Phys. Chemm Chem. Phys. **21**, 22849–22856 (2019)
28. L. Dagys et al., Nuclear hyperpolarization of (1–13C)-pyruvate in aqueous solution by proton-relayed side-arm hydrogenation. Analyst **146**, 1772–1778 (2021)
29. L. Kaltschnee et al., Hyperpolarization of amino acids in water utilizing parahydrogen on a rhodium nanocatalyst. Chem. Eur. J. **25**, 11031–11035 (2019)
30. J. McCormick et al., More than 12 % polarization and 20 minute lifetime of 15N in a choline derivative utilizing parahydrogen and a rhodium nanocatalyst in water. Angew. Chem. Int. Ed. **57**, 10692–10696 (2018)
31. S. Mamone et al., A field-independent method for the rapid generation of hyperpolarized [1–13C] pyruvate in clean water solutions for biomedical applications. Angew. Chem. Int. Ed. **61**, e202206298 (2022)
32. G. Stevanato et al., Real-time pyruvate chemical conversion monitoring enabled by PHIP. J. Am. Chem. Soc **145**, 5864–5871 (2023)
33. Y. Ding et al., Rapidly signal-enhanced metabolites for atomic scale monitoring of living cells with magnetic resonance. Chemistry-Methods **2**, e202200023 (2022)
34. P. Bhattacharya et al., Parahydrogen-induced polarization (PHIP) hyperpolarized MR receptor imaging in vivo: a pilot study of 13C imaging of atheroma in mice. NMR Biomed. **24**, 1023–1028 (2011)
35. M. Gierse et al., Parahydrogen-polarized fumarate for preclinical in vivo metabolic magnetic resonance imaging. J. Am. Chem. Soc. **145**, 5960–5969 (2023)
36. J.-B. Hövener et al., Parahydrogen-based hyperpolarization for biomedicine. Angew. Chem. Int. Ed. **57**, 11140–11162 (2018)
37. N.J. Stewart et al., Hyperpolarized 13C magnetic resonance imaging of fumarate metabolism by parahydrogen-induced polarization: a proof-of-concept in vivo study. ChemPhysChem **22**, 915–923 (2021)

38. L.M. Le Page, C. Guglielmetti, C.F. Najac, B. Tiret, M.M. Chaumeil, Hyperpolarized 13C magnetic resonance spectroscopy detects toxin-induced neuroinflammation in mice. NMR Biomed. **32**, e4164 (2019)
39. L.M. Le Page, C. Guglielmetti, C. Taglang, M.M. Chaumeil, Imaging brain metabolism using hyperpolarized 13C magnetic resonance spectroscopy. Trends Neurosci. **43**, 343–354 (2020)
40. E. Cavallari et al., The 13C hyperpolarized pyruvate generated by ParaHydrogen detects the response of the heart to altered metabolism in real time. Sci. Rep. **8**, 8366 (2018)
41. T. Hune et al., Metabolic tumor imaging with rapidly signal-enhanced 1–13C-pyruvate-d3. ChemPhysChem **24**, e202200615 (2023)
42. I. Park et al., Hyperpolarized 13C magnetic resonance metabolic imaging: application to brain tumors. Neuro Oncol. **12**, 133–144 (2010)
43. S. Düwel et al., Imaging of pH in vivo using hyperpolarized 13C-labelled zymonic acid. Nat. Commun **8**, 15126 (2017)
44. R.E. Hurd et al., Metabolic imaging in the anesthetized rat brain using hyperpolarized [1-13C] pyruvate and [1-13C] ethyl pyruvate. Magn. Reson. Med. **63**, 1137–1143 (2010)
45. R.E. Hurd et al., Cerebral dynamics and metabolism of hyperpolarized [1-13C]pyruvate using time-resolved MR spectroscopic imaging. J. Cereb. Blood Flow Metab. **30**, 1734–1741 (2010)
46. S.J. Nelson et al., DNP-hyperpolarized 13C magnetic resonance metabolic imaging for cancer applications. Appl. Magn. Reson. **34**, 533–544 (2008)
47. D.K. Hill et al., Model free approach to kinetic analysis of real-time hyperpolarized 13C magnetic resonance spectroscopy data. PLoS ONE **8**(9), e71996 (2013)
48. D.M. Spielman et al., In vivo measurement of ethanol metabolism in the rat liver using magnetic resonance spectroscopy of hyperpolarized [1-13C]pyruvate. Magn. Reson. Med. **62**, 307–313 (2009)
49. Y. Wen et al., Sex differences in kidney function and metabolism assessed using hyperpolarized [1-13C]pyruvate interleaved spectroscopy and nonspecific imaging. Tomography **6**, 5–13 (2020)
50. H. Lee et al., Determination of optimal scan time for the measurement of downstream metabolites in hyperpolarized 13C MRSI. IMRI **19**, 212–217 (2015)
51. R. Makaryus et al., The metabolomic profile during isoflurane anesthesia differs from propofol anesthesia in the live rodent brain. J. Cereb. Blood Flow Metab. **31**(6), 1432–1442 (2011)
52. S. Boretius et al., Halogenated volatile anesthetics alter brain metabolism as revealed by proton magnetic resonance spectroscopy of mice in vivo. Neuroimage **69**, 244–255 (2013)
53. A.B. Schmidt, M. Zimmermann, H. de Massin, C.A. Müller, V. Ivantaev, J. Hennig, Dv. Elverfeldt, J.-B. Hövener, Quasi-continuous production of highly hyperpolarized carbon-13 contrast agents every 15 seconds within an MRI system. Commun. Chem. **5**, 21 (2022)

Authors and Affiliations

Theresa L. K. Hune[1,2] · Salvatore Mamone[1,2] · Andreas B. Schmidt[3,4,5] · Inês Mahú[6] · Natascha D'Apolito[7] · Dirk Wiedermann[7] · Jens Brüning[6] · Stefan Glöggler[1,2]

✉ Stefan Glöggler
stefan.gloeggler@mpinat.mpg.de

[1] NMR Signal Enhancement Group, Max Planck Institute for Multidisciplinary Sciences, Göttingen, Germany

[2] Center for Biostructural Imaging of Neurodegeneration of the University Medical Center Göttingen, Göttingen, Germany

[3] Division of Medical Physics, Department of Radiology, Faculty of Medicine, Medical Center, University of Freiburg, Killianstr. 5a, 79106 Freiburg, Germany

[4] German Cancer Research Center (DKFZ), German Cancer Consortium (DKTK), Partner Site Freiburg, Im Neuenheimer Feld 280, 69120 Heidelberg, Germany

[5] Department of Chemistry, Integrative Biosciences (Ibio), Karmanos Cancer Institute (KCI), Wayne State University, Detroit, MI 48202, USA

[6] Department of Neuronal Control of Metabolism, Max Planck Institute for Metabolism Research, Gleueler Straße 50, 50931 Cologne, Germany

[7] Multimodal Imaging Group, Max Planck Institute for Metabolism Research, Gleueler Straße 50, 50931 Cologne, Germany